

Simultaneous sub-Doppler laser cooling of fermionic ${}^6\text{Li}$ and ${}^{40}\text{K}$ on the D_1 line: Theory and experiment

Franz Sievers,^{1,*} Norman Kretschmar,¹ Diogo Rio Fernandes,¹ Daniel Suchet,¹ Michael Rabinovic,¹ Saijun Wu,^{2,†} Colin V. Parker,³ Lev Khaykovich,⁴ Christophe Salomon,¹ and Frédéric Chevy¹

¹Laboratoire Kastler Brossel, École Normale Supérieure, CNRS, UPMC, 24 rue Lhomond, 75005 Paris, France

²State Key Laboratory of Surface Physics and Department of Physics, Fudan University, 200433 Shanghai, People's Republic of China

³James Franck Institute, Enrico Fermi Institute and Department of Physics, University of Chicago, Chicago, Illinois 60637, USA

⁴Department of Physics, Bar-Ilan University, Ramat-Gan 52900, Israel

(Received 30 October 2014; revised manuscript received 30 January 2015; published 23 February 2015)

We report on simultaneous sub-Doppler laser cooling of fermionic ${}^6\text{Li}$ and ${}^{40}\text{K}$ using the D_1 optical transitions. We compare experimental results to a numerical simulation of the cooling process applying a semiclassical Monte Carlo wave-function method. The simulation takes into account the three-dimensional optical molasses setup and the dipole interaction between atoms and the bichromatic light field driving the D_1 transitions. We discuss the physical mechanisms at play, identify the important role of coherences between the ground-state hyperfine levels, and compare D_1 and D_2 sub-Doppler cooling. In 5 ms, the D_1 molasses phase greatly reduces the temperature for both ${}^6\text{Li}$ and ${}^{40}\text{K}$ at the same time, with final temperatures of 44 and 11 μK , respectively. For both species this leads to a phase-space density close to 10^{-4} . These conditions are well suited to direct loading of an optical or magnetic trap for efficient evaporative cooling to quantum degeneracy.

DOI: [10.1103/PhysRevA.91.023426](https://doi.org/10.1103/PhysRevA.91.023426)

PACS number(s): 37.10.De, 32.80.Wr, 67.85.-d

I. INTRODUCTION

The road towards quantum degeneracy in atomic gases usually starts with a laser cooling and trapping phase. The resulting initial phase-space density of the atomic ensemble and the initial collision rate should be as high as possible for initiating efficient evaporative cooling to quantum degeneracy. Sub-Doppler cooling has proven to be a powerful technique to increase the phase-space density of most alkali atoms and other atoms with multiple-level structure [1–3]. However, in the case of lithium and potassium, the narrow excited-state structure of the D_2 transition compromises the efficiency of this cooling scheme [4,5]. Both species possess stable fermionic and bosonic isotopes, and they play an important role in recent experimental studies of strongly correlated quantum gases. Thus, important efforts have been devoted to searching for alternative laser cooling schemes.

For instance, it has recently been shown that three-dimensional (3D) Sisyphus cooling for ${}^7\text{Li}$, some gigahertz red detuned from the D_2 line, can lead to temperatures as low as 100 μK , with up to 45% of the atoms in the cooled fraction [6]. A second option is to operate the magneto-optical trap (MOT) on a transition with a smaller linewidth to reduce the Doppler temperature [7–9]. Such transitions exist for ${}^6\text{Li}$ and ${}^{40}\text{K}$ in the near-UV and blue regions of the spectrum, respectively, leading to temperatures of 33 μK for ${}^6\text{Li}$ and 63 μK for ${}^{40}\text{K}$. Yet, special optics and a coherent source at 323 nm for ${}^6\text{Li}$ and at 405 nm for ${}^{40}\text{K}$ are needed for this approach. Additionally, at these wavelenghtes the available power is still a limiting factor.

More recently a simpler sub-Doppler cooling scheme using blue-detuned molasses operating on the D_1 line was proposed and demonstrated on ${}^{40}\text{K}$ [10] and has been extended to other

atomic species such as ${}^7\text{Li}$ [11], ${}^{39}\text{K}$ [12,13], and ${}^6\text{Li}$ [14]. Using this technique, temperatures as low as 20 μK (${}^{40}\text{K}$), 50 μK (${}^7\text{Li}$), 6 μK (${}^{39}\text{K}$), and 40 μK (${}^6\text{Li}$) were reached.

Even though the main ingredients of the D_1 cooling scheme are now understood at a qualitative level, in particular, the role of the coherences between hyperfine ground-state levels [11], a complete picture, taking into account the full level structure of the atoms, is still missing. In this paper, we present a 3D semiclassical solution of the optical Bloch equations that takes into account the full set of relevant energy levels of alkali atoms and we apply it to the case of ${}^6\text{Li}$ and ${}^{40}\text{K}$. The model fully confirms the experimentally observed cooling behavior and its robustness with respect to changes in experimental parameters. The model is validated by a good match between the simulation and the experimentally measured temperature and fluorescence rate. We recover the important role of the Raman detuning between the main cooling laser and the repumping laser on the achievable temperature. We show here, for both ${}^6\text{Li}$ and ${}^{40}\text{K}$, that the gain in temperature of a factor of ~ 3 at the exact Raman resonance is well reproduced by the theoretical model and that the amount of coherence between both hyperfine states shows a pronounced resonance behavior. Beyond individual studies of the two species, we also show experimentally that simultaneous cooling of ${}^6\text{Li}$ and ${}^{40}\text{K}$ does not lead to any severe trade-off and is technically easy to implement. We are able to capture more than 1×10^9 atoms of each species, with a capture efficiency exceeding 60% from a compressed magneto-optical trap (CMOT), and reach temperatures as low as 44 μK for ${}^6\text{Li}$ and 11 μK for ${}^{40}\text{K}$ within 5 ms.

II. D_1 COOLING MECHANISM

In a typical D_1 cooling setup (Fig. 1), all the D_1 hyperfine levels are involved in the interaction. The sub-Doppler cooling effects include a mix of Sisyphus cooling, motion-induced and off-resonant light coupling from gray to bright levels, and

*franz.sievers@lkb.ens.fr

†saijunwu@fudan.edu.cn

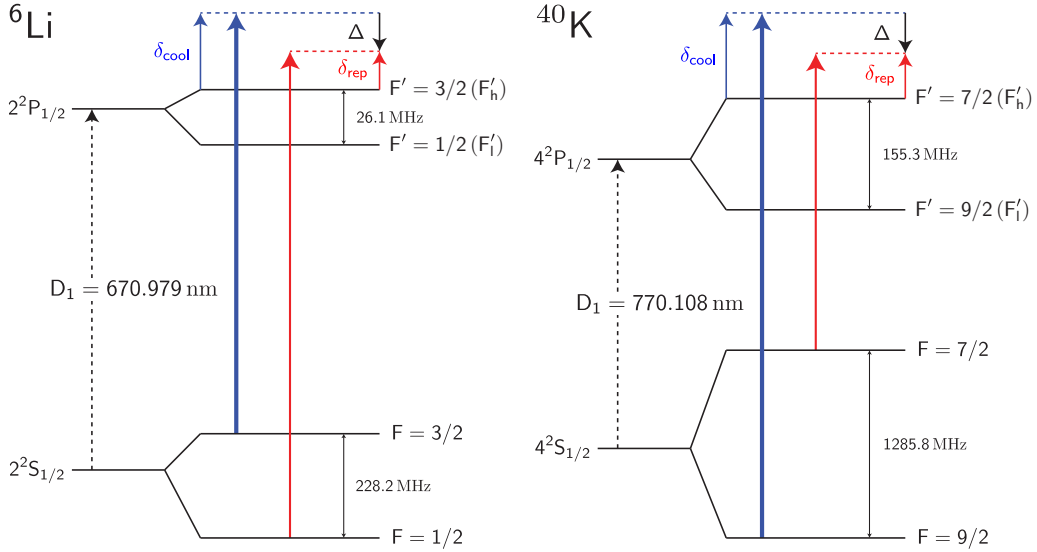


FIG. 1. (Color online) Cooling scheme on the ${}^6\text{Li}$ and ${}^{40}\text{K}$ D_1 lines. The cooling beam (blue) is blue detuned by δ_{cool} from the $|F = 3/2\rangle \rightarrow |F'_h = 3/2\rangle$ ($|F = 9/2\rangle \rightarrow |F'_h = 7/2\rangle$) transition, where F'_h (F'_l) is the upper (lower) excited-state level. The repumping beam (red) is blue detuned by δ_{rep} from the $|F = 1/2\rangle \rightarrow |F'_h = 3/2\rangle$ ($|F = 7/2\rangle \rightarrow |F'_h = 7/2\rangle$) transition. Detuning from the Raman condition is denoted $\Delta = \delta_{\text{rep}} - \delta_{\text{cool}}$.

coherent population trapping of slow atoms in nearly decoupled states. In this section we first introduce our semiclassical laser cooling model. We then present and compare the results from experimental observations and numerical simulations and, finally, discuss the physical mechanism of D_1 cooling.

A. Semiclassical Monte Carlo simulation

The level diagrams of our bichromatic cooling scheme for both ${}^6\text{Li}$ and ${}^{40}\text{K}$ are depicted in Fig. 1. The D_1 molasses is composed of a 3D lattice whose polarization configuration is the same as that of a six-beam standard MOT, but with two sidebands to address the $|F = 3/2\rangle$ and $|F = 1/2\rangle$ hyperfine ground states of ${}^6\text{Li}$ (respectively, $|F = 9/2\rangle$ and $|F = 7/2\rangle$) for ${}^{40}\text{K}$) in the D_1 Λ system at positive detunings.

Here, by convention, we refer to the $|F = 3/2\rangle \rightarrow |F'_h\rangle$ and $|F = 1/2\rangle \rightarrow |F'_h\rangle$ transitions as cooling and repumping transitions. It is, however, important to note that neither the cooling nor the repumping D_1 transitions are actually closed.

Our numerical simulation of the cooling process is based on a semiclassical Monte Carlo wave-function method. The simulation takes into account the 3D optical molasses setup and the dipole interaction between the single atoms and the polarized light driving the transitions of the D_1 manifold, which is spanned by the $4(2I + 1)$ hyperfine Zeeman sublevels ($I > 0$ is the nuclear spin). We treat the external states of the atom classically and update its position $\mathbf{r}(t)$ and velocity $\mathbf{v}(t)$ according to the calculated expectation value of the light force:

$$\dot{\mathbf{f}}(t) = \frac{\langle \psi(t) | -\nabla H_{\text{eff}}(\mathbf{r}(t)) | \psi(t) \rangle}{\langle \psi(t) | \psi(t) \rangle}. \quad (1)$$

The atomic internal states $|\psi(t)\rangle$ evolve in a dressed basis with respect to the cooling laser (Fig. 1), according to the Monte Carlo wave-function method [15,16] with the effective rotating-wave Hamiltonian

$$H_{\text{eff}} = H_0 + H_{F=I-1/2} + H_{F=I+1/2} - i\hat{\Gamma}/2, \quad (2)$$

where

$$H_0 = \sum_m |F = I - 1/2, m\rangle \hbar \Delta \langle F = I - 1/2, m| - \sum_{F', m'} |F', m'\rangle \hbar (\delta_{\text{cool}} + \delta_{\text{hfs}, F'}) \langle F', m'|. \quad (3)$$

Here H_0 operates over the whole D_1 manifold and δ_{cool} is the detuning of the cooling laser with respect to the $F = I + 1/2 \rightarrow F'_h$ transition, where F'_h (Fig. 1) corresponds to the excited hyperfine level that is higher in energy, e.g., $F'_h = 3/2$ for ${}^6\text{Li}$ and $F'_h = 7/2$ for ${}^{40}\text{K}$. $\Delta = \delta_{\text{rep}} - \delta_{\text{cool}}$ is the two-photon detuning for the $F = I - 1/2 \rightarrow F = I + 1/2$ Raman transition, $\delta_{\text{hfs}, F'}$ the hyperfine splitting of the excited state for F'_l , and 0 for F'_h . The 0 of energy is chosen as that of the bare $F = I + 1/2$ ground state.

The light-atom coupling Hamiltonian

$$H_{F=I\pm 1/2} = \hbar \sum_{m, \sigma, F', m'} \Omega_{F, \sigma} c_{F, m, \sigma, F', m'} \times |F, m\rangle \langle F', m'| + \text{H.c.} \quad (4)$$

describes the cooling ($F = I + 1/2$) and repumping ($F = I - 1/2$) interactions [17]. Here $\Omega_{F, \sigma}$ are the Rabi frequencies of the repumping and cooling laser beams for $F = I - 1/2$ $F = I + 1/2$, respectively. $c_{F, m, \sigma, F', m'}$ represent the Clebsch-Gordan coefficients associated with the transitions coupled by σ polarized light. To take into account the radiation damping we include the spontaneous emission rate $\hat{\Gamma} = \Gamma \hat{P}_{ee}$ where Γ is the excited-state linewidth and $\hat{P}_{ee} = \sum_{F', m'} |F', m'\rangle \langle F', m'|$. This leads to a decay of the internal-state wave-function norm $\langle \psi(t) | \psi(t) \rangle$. The speed of this decay probabilistically dictates the collapse of the internal quantum states in the numerical simulation, which corresponds to spontaneous emission. We take into account the polarization of the spontaneous scattering photon and follow the standard quantum jump procedure to project the atomic states to ground states, with the norm

reset to unity [15]. To effectively account for heating due to both absorption and spontaneous emission, we assign a recoil momentum shift to $\mathbf{v}(t)$ twice before continuing to evolve $|\psi(t)\rangle$ via $H_{\text{eff}}(\mathbf{r}(t))$.

The simulations are performed with parameters matching the experimental setup by properly introducing the spatially dependent $\Omega_{F,\sigma}(\mathbf{r})$, the detunings Δ , δ_{cool} , and atomic initial conditions. To reproduce experimental conditions, we fix the relative phases for all 12 cooling and repumping laser beams at values randomized for each simulation trial. We record the evolution of the 3D atomic velocity, the time-stamped fluorescence events corresponding to quantum jumps, and internal-state properties such as state population and coherence. The observables are averaged over multiple simulation trials for comparison with the experiment.

B. Raman-detuning dependence for ${}^6\text{Li}$

A critical parameter in the D_1 molasses scheme is the Raman detuning Δ (Fig. 1). In the following we investigate the Raman-detuning dependence of the ${}^6\text{Li}$ molasses temperature and fluorescence rate both theoretically and experimentally, for various cooling and repumping laser intensities.

Our ${}^6\text{Li}$ - ${}^{40}\text{K}$ machine is described in [18]. We first load a lithium MOT using a laser-slowed atomic beam (Zeeman slower). After a compressed MOT phase the magnetic field and the D_2 light are switched off and the D_1 molasses is applied

(a more detailed description of the sequence is presented in the Appendix). To probe the Raman-detuning dependence we apply a $100\text{-}\mu\text{s}$ D_1 molasses pulse with variable Δ to an atomic cloud precooled to $100\text{ }\mu\text{K}$. Figures 2(a) and 2(b) show the fluorescence rate and the temperature after the pulse as functions of the Raman detuning Δ for the intensities used in the simulations. We observe a temperature dip at zero Raman detuning and a heating and fluorescence peak at positive Δ whose position and amplitude are correlated with the molasses intensity.

In the simulations we set the initial velocity of lithium to 0.2 m/s ($T \sim 30\text{ }\mu\text{K}$). The simulation time is set to $200\text{ }\mu\text{s}$. In the first $100\text{ }\mu\text{s}$ we allow the cooling dynamics to equilibrate, and during the second $100\text{ }\mu\text{s}$ we record the velocity $\mathbf{v}(t)$ as well as the time-stamped quantum jump events to calculate the equilibrium temperature and fluorescence rate. At each Raman detuning we average over 25 trajectories. The simulation results for two intensities, $I_{\text{cool}} = 2.7 I_{\text{sat}}$, $I_{\text{rep}} = 0.13 I_{\text{sat}}$ and $I_{\text{cool}} = 9 I_{\text{sat}}$, $I_{\text{rep}} = 0.46 I_{\text{sat}}$, are shown in Figs. 2(c) and 2(d), respectively (here I_{sat} refers to the saturation intensity of the D_2 line).

The simulated heating and fluorescence peak positions for low and high intensities (Fig. 2) agree well with the experimental findings. Also, the shift between the heating and the fluorescence peak, which increases with the molasses intensity, is numerically reproduced without any freely adjustable parameters.

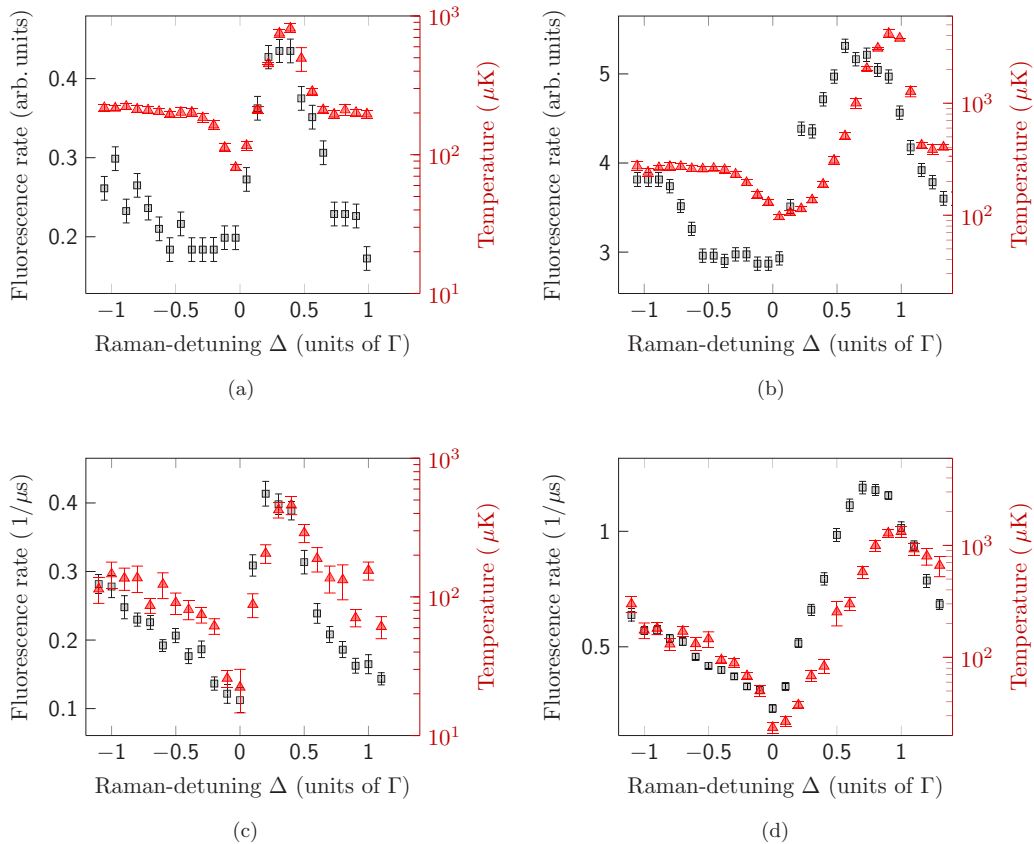


FIG. 2. (Color online) Fluorescence (squares) and temperature (triangles; logarithmic scale) of the ${}^6\text{Li}$ atomic cloud after a $100\text{-}\mu\text{s}$ pulse of D_1 light with variable Raman detuning Δ . Experiment: (a) low intensity; (b) high intensity. Simulation: (c) low intensity; (d) high intensity. Experimental and simulation results (a, c) for $I_{\text{cool}} = 2.7 I_{\text{sat}}$, $I_{\text{rep}} = 0.13 I_{\text{sat}}$ and (b, d) for $I_{\text{cool}} = 9 I_{\text{sat}}$, $I_{\text{rep}} = 0.46 I_{\text{sat}}$ per beam.

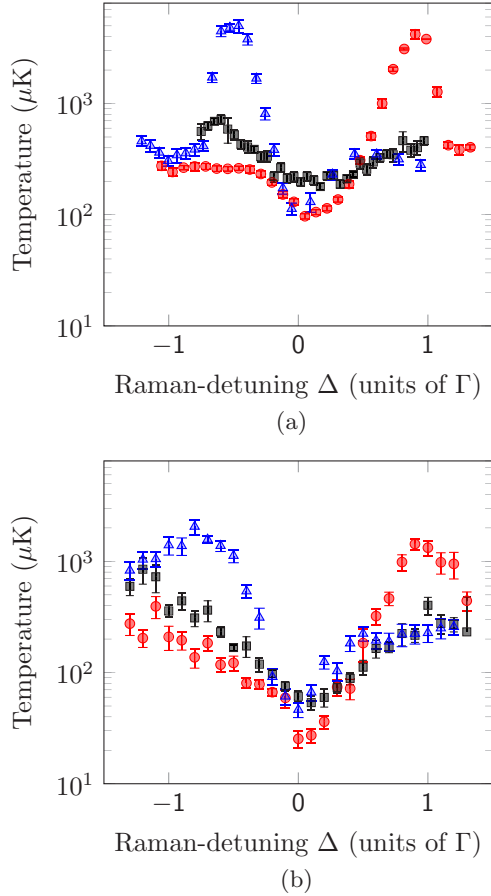


FIG. 3. (Color online) Temperature of the ${}^6\text{Li}$ D_1 molasses after a $100\text{-}\mu\text{s}$ pulse with variable Raman detuning Δ for different cooling and repumping intensities. (a) Experiment; (b) simulation. Standard intensities [(red) circles]: $I_{\text{cool}} = 9 I_{\text{sat}}$, $I_{\text{rep}} = 0.46 I_{\text{sat}}$. Equal cooling/repumping ratio (black squares): $I_{\text{cool}} = I_{\text{rep}} = 9 I_{\text{sat}}$. Inverted cooling/repumping ratio [(blue) triangles]: $I_{\text{cool}} = 0.6 I_{\text{sat}}$, $I_{\text{rep}} = 4.6 I_{\text{sat}}$.

Despite the nice match between simulations and experiments in Figs. 2 and 3, we observe that the semiclassical simulations provide temperatures that are systematically lower by a factor of 2 to 4 than the measured ones, particularly near the Raman-resonance condition $\Delta = 0$. Here the simulation predicts a temperature of $20\ \mu\text{K}$, whereas the lowest measured temperature is $50\ \mu\text{K}$. The reason for this is not fully understood and may come from both theory and experimental limitations. First, the simulation is semiclassical and neglects the wave-function extent of the cold atoms. The predicted temperature of $20\ \mu\text{K}$ corresponds to only six times the recoil energy $E_R = \frac{1}{2} m v_{\text{recoil}}^2 = k_B \times 3.5\ \mu\text{K}$. Therefore, only a quantum treatment of the atoms' external motion can be expected to give a quantitative equilibrium temperature prediction in the low-intensity limit. In the simulation we observe that slow atoms are likely trapped within subwavelength regions, where the light shift is minimal and the atom is nearly decoupled from light over a long time without quantum jump. This coherent population trapping effect enhances the cooling at both large and small Δ , although it is most pronounced at the Raman resonance ($\Delta = 0$) since more choices of decoupled

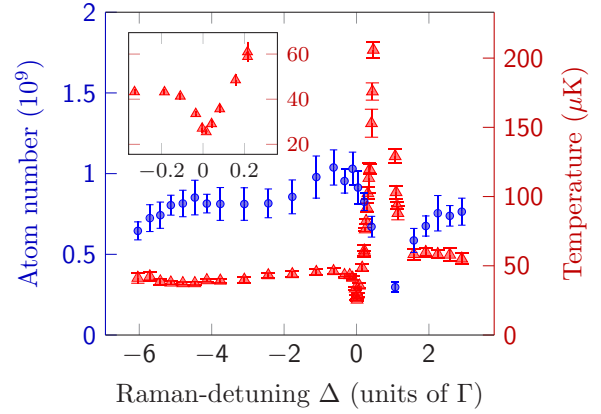


FIG. 4. (Color online) Experiment: Atom number and equilibrium temperature of the ${}^{40}\text{K}$ D_1 molasses as functions of the Raman detuning Δ . $\delta_{\text{cool}} = 3\ \Gamma$, $I_{\text{cool}} = 6 I_{\text{sat}}$, $I_{\text{rep}}/I_{\text{cool}} = 7.6\%$, $t_m = 5\ \text{ms}$. In the constant-temperature regions below $-0.1\ \Gamma$ and above $2\ \Gamma$ gray molasses cooling involves coherences between Zeeman states in a given hyperfine state but not between hyperfine states. At the exact Raman condition $\Delta = 0$, long-lived coherences between hyperfine states are established, as shown in the simulation in Fig. 5. In a narrow detuning range, the temperature [(red) triangles] drops to $20\ \mu\text{K}$. Inset: Expanded scale.

states emerge. The semiclassical picture clearly exaggerates the cooling effect since the wave nature of the atoms' external motion is not included in the model. In fact, the wave function of the slow atoms will sample a larger volume of the subwavelength traps and will shorten the lifetime of the dark periods.

On the experimental side the residual magnetic field cancellation has only been coarsely tuned for the data set presented in Fig. 2 (as well as in Figs. 3 and 4). With careful tuning of the magnetic field zeroing we were able to lower the ${}^{40}\text{K}$ temperature to $11\ \mu\text{K}$ (Sec. II C, on ${}^{40}\text{K}$) for lower-density samples. Interestingly, other groups have indeed found on ${}^{39}\text{K}$ lower temperatures ($6\ \mu\text{K}$) than ours under the Raman condition [12]. Note also that in Fig. 2 for positive Raman detunings ($\Delta \sim 0.5\ \Gamma$ at low intensity and $\Delta \sim \Gamma$ at high intensity) the “temperature” corresponds to out-of-equilibrium situations as the atoms are quickly heated away and lost from the molasses. The notion of temperature should thus be taken with care in this region, unlike for negative Raman detunings, where a steady-state temperature is reached.

Another reason for shortening the lifetime of dark periods of the slow atoms is reabsorption of photons emitted by other atoms. We have indeed seen a density-dependent excess temperature, which we measured to be $4.6\ \mu\text{K} \times 10^{11}$ at cm^3 for ${}^{40}\text{K}$. A careful simulation of cooling including photon reabsorption processes is far more complex and is beyond the scope of this work.

We also study the same Raman-detuning-dependent effects, but for different cooling/repumping ratios. Typical experimental and simulation results are presented in Fig. 3. Here again, the simulation parameters are chosen according to the experimental values. The simulation and experiments match fairly well. In particular, for the usual configuration with $I_{\text{cool}}/I_{\text{rep}} > 1$ ($I_{\text{cool}} = 9 I_{\text{sat}}$ and $I_{\text{rep}} = 0.45 I_{\text{sat}}$), we observe a

heating peak at $\Delta > 0$. When inverting the roles of the cooling and repumping light, i.e., $I_{\text{cool}}/I_{\text{rep}} < 1$ ($I_{\text{cool}} = 0.6I_{\text{sat}}$ and $I_{\text{rep}} = 4.6I_{\text{sat}}$), the heating peak appears for $\Delta < 0$ instead. In all cases, cooling is most efficient at the Raman resonance ($\Delta = 0$). Finally, for I_{cool} equal to I_{rep} , both as large as $9I_{\text{sat}}$, we observe less efficient cooling at $\Delta = 0$, with moderate heating at blue and red detunings.

C. Raman-detuning dependence for ^{40}K

Typical simulation results for ^{40}K are shown in Fig. 5(a). Compared to ^6Li , simulations for ^{40}K require a significantly higher computational power due to the larger internal-state dimensions as well as the larger atomic mass and therefore slower cooling dynamics. To save computation time, we start at a velocity of 0.2 m/s ($T \sim 50 \mu\text{K}$) and set the simulation time to 2 ms. We record the velocity $\mathbf{v}(t)$ as well as the time-stamped quantum jump events for $t > 1$ ms to calculate the fluorescence rate. For each Raman detuning Δ , 13 trajectories are simulated.

Experimental results for ^{40}K are presented in Fig. 4, which shows the temperature and atom number of the D_1 molasses as functions of the Raman detuning Δ . The total molasses

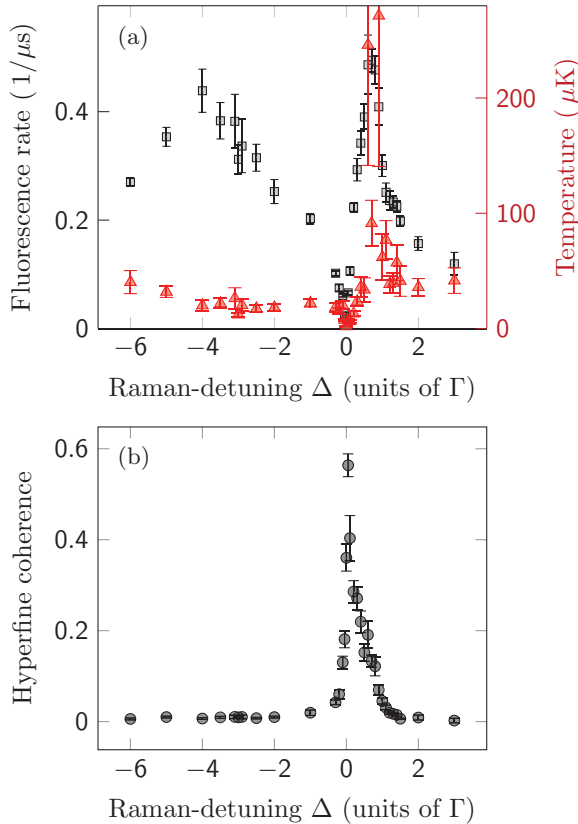


FIG. 5. (Color online) Simulation: Hyperfine coherence and Λ -enhanced cooling for the ^{40}K D_1 molasses. Simulation time, 2 ms; $\delta_{\text{cool}} = 3 \Gamma$; $I_{\text{cool}} = 6I_{\text{sat}}$; $I_{\text{rep}}/I_{\text{cool}} = 7.6\%$. (a) Fluorescence (squares) and temperature (triangles) as functions of the Raman detuning Δ . (b) Coherence $4 \cdot \langle \rho_{F=7/2, F=9/2}^2 \rangle$ between the two hyperfine ground states, $F = 7/2$ and $F = 9/2$ (see Sec. III E). The coherence is peaked under the Raman-resonance condition, with a width matching the temperature dip.

duration $t_m = 5$ ms. In the last 2 ms a linear intensity ramp to $I_{\text{cool}} = 6I_{\text{sat}}$ is performed. Just like ^6Li , we observe a sharp temperature drop under the Raman condition, a heating resonance at $\sim 0.7 \Gamma$, and constant-temperature regions below -0.1Γ and above 2Γ . For the constant-temperature regions the temperature $T \sim 45 \mu\text{K}$ is low compared to the Doppler temperature $T_{\text{Doppler, K}} = 145 \mu\text{K}$. Under the Raman condition the temperature decreases to $23 \mu\text{K}$. Under carefully optimized conditions we measured temperatures as low as $11 \mu\text{K}$.

As for ^6Li , the comparison between Fig. 4 and Fig. 5(a) again demonstrates the qualitative agreement between simulations and experimental results and that the heating peak position is reproduced by the simulation without adjustable parameters. Interestingly, the inverted hyperfine structure in the ground and excited states of ^{40}K and the different $F \rightarrow F' = F - 1$ transition for the cooling laser and $F \rightarrow F' = F$ repumping transition does not significantly modify the D_1 cooling scheme compared to ^6Li .

D. The D_1 cooling mechanism

The agreement between simulation and experiment suggests that the semiclassical picture is able to catch the essential physics behind the D_1 molasses cooling. In particular, the mechanisms behind the cooling dips and heating peaks in Figs. 2 to 4, previously interpreted using the dressed atom picture with a simplified three-level model [11], survive in the full level scheme of the D_1 transition.

It is well known that efficient D_2 sub-Doppler cooling requires isolated excited hyperfine levels for alkaline atoms [4,5]. In contrast, D_1 gray molasses operates well even when all D_1 levels are excited (as in the case of ^6Li) and even at zero excited-state hyperfine splitting as confirmed numerically. The robustness of D_1 molasses is also seen in its insensitivity to the relative phase between the “cooling” and the “repumping” lattices, a critical parameter for D_2 bichromatic cooling where no polarization gradient was introduced [19].

In the following we discuss the physics behind the robustness of the D_1 sub-Doppler cooling. We then revisit the cooling dips and heating peaks in Figs. 2 to 4.

We note that all the dipole-allowed D_1 transitions (Fig. 1) are “open”: when addressed with weak off-resonant light, the probability of inelastic (m_F - or F -changing) photon scattering is comparable to or higher than that of elastic scattering. When blue detuned from the D_1 transitions, an off-resonant bichromatic lattice can establish a correlation between the spatially varying light shift (due to virtual elastic scattering) and decay (due to real inelastic scattering) for the dressed ground states, since a larger light shift is accompanied by a stronger light-atom coupling and typically a larger inelastic scattering cross section.

We verify this idea with the full D_1 model for ^6Li atoms subjected to a 1D lattice with orthogonal linear polarizations (lin \perp lin configuration) with typical cooling parameters. The spatially varying light shifts ϵ of the six dressed ground states of ^6Li are plotted in Fig. 6(a). The decay of the dressed states, due to inelastic light scattering, is characterized by the decay rate γ , which is plotted versus ϵ in Fig. 6(d). We see a correlation between ϵ and γ for $\epsilon < 1.5$ MHz. This correlation is robustly established for the D_1 transitions, as

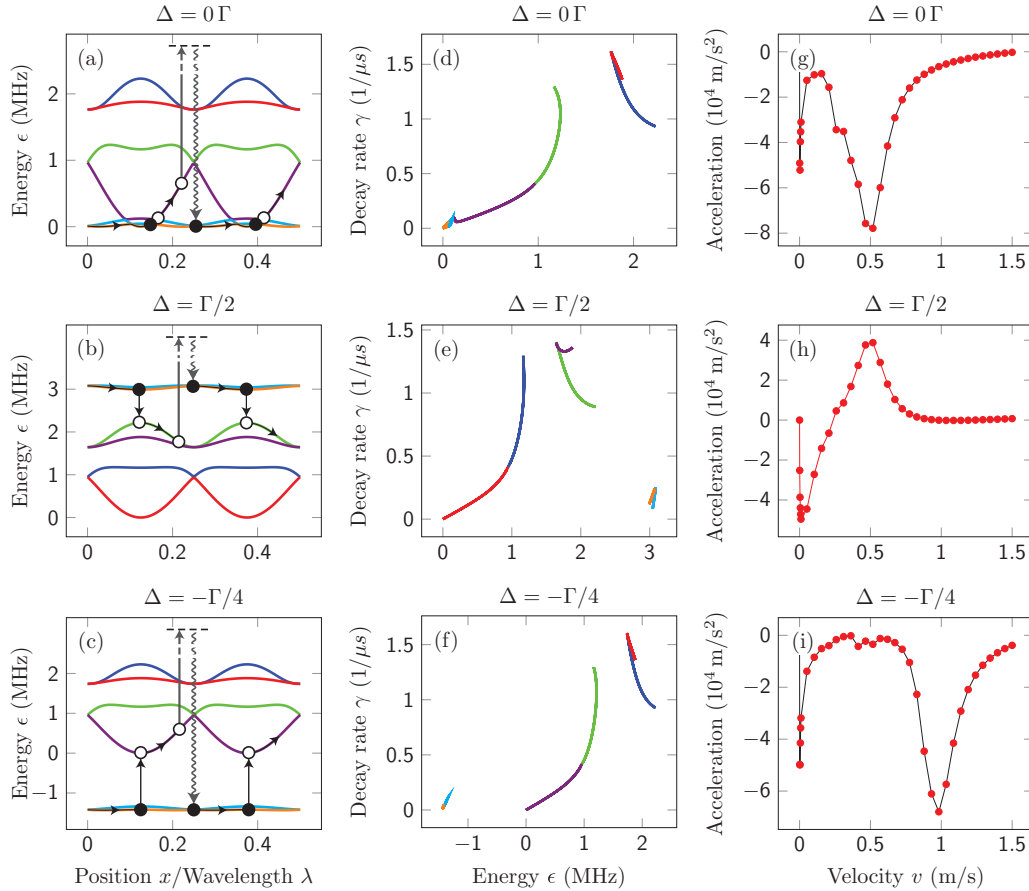


FIG. 6. (Color online) Cooling mechanism around the Raman condition in a simplified model. Optical Bloch equation simulation for ${}^6\text{Li}$ subjected to a 1D bichromatic lattice with linear orthogonal polarizations near D_1 resonance. The cooling lattice and repumping lattice are displaced by π ($\lambda/4$). $I_{\text{cool}} = 15I_{\text{sat}}$, $I_{\text{rep}} = 0.75I_{\text{sat}}$, $\delta_{\text{cool}} = 4\Gamma$. (a–c) Dressed states as functions of the position, in units of the D_1 optical wavelength. The two dressed $F = 1/2$ levels (light blue and orange) are nearly flat in all the graphs due to the small I_{rep} . (d–f) Decay rate of dressed states as a function of their energy shifts. Here the two dressed $F = 1/2$ levels span a very small energy range and have a low decay rate. (g–i) Velocity-dependent optical force for an atom dragged at velocity v . (a, d, g) $\Delta = 0$; (b, e, h) $\Delta = \Gamma/2$; (c, f, i) $\Delta = -\Gamma/4$. Note the negative sign of the force in (g) and (i), implying cooling, and the anticooling force for velocities near 0.5 m/s in (h).

verified numerically in the more complicated 3D lattices and for other atomic species. The correlation even persists for a fictitious atom with vanishing D_1 hyperfine splitting and reduced m_F -changing light scattering [20].

Such a correlation between the spatially dependent light shift ϵ and decay rate γ has two consequences: First, atoms with $kv < \gamma$ tend to accumulate in dressed states with low light shifts, which facilitates cooling through motion-induced coupling to higher energy dressed states [21]. This coupling is nonadiabatic as in the famous $\sigma^+ - \sigma^-$ 1D velocity selective coherent population trapping subrecoil cooling mechanism (VSCPT), where the spatial gradient of the atomic wave function induces a coupling to a bright state. Second, for a slowly moving atom that adiabatically follows a particular dressed state, the atom tends to leave the dressed state when the light shift is high, leading to Sisyphus cooling. In addition, at locations where $\epsilon, \gamma \sim 0$, slow atoms can be confined near the local dark states such as those in Fig. 6(a) near $x = 0, \lambda/8, \lambda/4, 3\lambda/8$ [22]. The resulting optical cooling force is plotted in Fig. 6(g) and is negative (cooling effect) over a broad range. We emphasize that this simplified 1D analysis remains valid in the more complex 3D beam geometry

and is not restricted to ${}^6\text{Li}$ atoms. The D_1 laser cooling mechanism applies to all alkalis, even those amenable to efficient D_2 sub-Doppler cooling such as cesium and rubidium. As D_1 laser cooling involves dark states, it is less affected by density-dependent photon multiple scattering and heating than D_2 sub-Doppler cooling. Therefore it would be interesting to quantify the gain in phase-space density by applying D_1 sub-Doppler cooling for these atoms.

In comparison, sub-Doppler cooling on the D_2 lines is significantly different. While the $F = I \pm 1/2 \rightarrow F' = I \pm 1/2$ transitions are as “open” as in D_1 , the $F = I + 1/2 \rightarrow F' = I + 3/2$ and $F = I - 1/2 \rightarrow F' = I - 3/2$ transitions have both “closed” and open transitions. Here the closed transitions are characterized by a greater-than-unity elastic-to-inelastic scattering ratio. If the $F = I + 1/2 \rightarrow F' = I + 3/2$ transitions can be isolated, then by taking advantage of the nearly closed $m_F - m_{F'}$ transitions, a correlation between the light shift and the decay rate can be established with (instead) a red-detuned lattice, as in standard sub-Doppler cooling [1–3]. However, in the case of small hyperfine splitting the open hyperfine transitions are as well addressed at red detuning, leading to short-lived potential minima and

degraded correlations, contributing to the inefficiency of the sub-Doppler cooling [23].

E. Physical picture of the Raman-detuning effect

We now extend the three-level picture in Ref. [11] to understand the details of the experiment. The cooling dips observed both experimentally and numerically under the Raman-resonance condition are also fairly easy to understand in the full model: At $\Delta = 0$ the resonant Raman-coupling splits the $F = I \pm 1/2$ hyperfine ground states into a bright and a dark manifold. The dark manifold is weakly coupled to the molasses. More precisely, the coupling strength of the Raman dark manifold is even weaker than those due to individual cooling-repumping couplings. Therefore the emergence of the Raman dark manifold enhances all sub-Doppler cooling effects.

Since the dark manifold is a coherent superposition of the two hyperfine states $F_1 = I - 1/2$ and $F_2 = I + 1/2$, we expect that laser-cooled atoms mostly occupy the dark manifold and therefore display a hyperfine coherence ρ_{F_1, F_2} with significant amplitude. To test this picture, we record the time-dependent off-diagonal density matrix quantity $4 \cdot \langle \rho_{F_1, F_2}^2(t) \rangle$ for all the quantum trajectories of the numerical simulations. The factor 4 ensures the normalization to one for the maximally coherent situation. To compute the two-photon detuning Δ -dependent quantity $4 \cdot \langle \rho_{F_1, F_2}^2 \rangle$, we average over both the equilibrium time and many quantum trajectories at fixed Δ . Typical results for ^{40}K are given in Fig. 5, with the cooling parameters corresponding to Fig. 4. We see that the coherence $4 \cdot \langle \rho_{F_1=7/2, F_2=9/2}^2 \rangle$ is peaked under the Raman-resonance condition and becomes significant, with a width matching the temperature dip.

As in Figs. 2 to 4 and [11] we now explain the heating peaks with the full D_1 model. We first focus on the case of $I_{\text{cool}} \gg I_{\text{rep}}$ so that at large $|\Delta|$ the dressed $F = I - 1/2$ hyperfine level is relatively long-lived and populated. As shown in Figs. 6(b) and 6(c), the Raman detuning Δ determines the energy level of the dressed $F = I - 1/2$ hyperfine level, and it is clear that when $\Delta < 0$, the motion-induced coupling to the dressed $F = I + 1/2$ level should still contribute to cooling [as in Figs. 6(c), 6(f), and 6(i)] [21], apart from Sisyphus cooling. On the contrary, for $\Delta > \max[\epsilon_{F=I+1/2}]$, e.g., a Raman detuning beyond the maximum light shift of the dressed $F = I + 1/2$ manifold [as in Figs. 6(b), 6(e), and 6(h)], motion-induced coupling to the lower energy dressed $F = I + 1/2$ manifold would lead to heating. In addition, the Sisyphus effect at the $F = I + 1/2$ manifold also contributes to heating, since atoms coupled from $F = I - 1/2$ are more likely to start at the antitrap positions. The corresponding heating peak is located at $\Delta \sim \max[\epsilon_{F=I+1/2}] > 0$.

When $I_{\text{cool}} \ll I_{\text{rep}}$, the heating peak is shifted to $\Delta \sim -\max[\epsilon_{F=I-1/2}] < 0$, as in Fig. 3. This is straightforward to understand, as the roles of the two hyperfine ground states are now inverted with respect to the previous case. Finally, for $I_{\text{cool}} \sim I_{\text{rep}}$, the two hyperfine ground states have similar lifetimes and therefore similar steady-state populations. As the heating effects are balanced by cooling effects, the corresponding heating peaks in Fig. 3 (black squares) at

TABLE I. Parameters of the simultaneous ^6Li and ^{40}K D_1 cooling phase.

Parameter	Potassium	Lithium
P (mW)	230	300
δ_{cool} (Γ)	2.3	4
δ_{rep} (Γ)	2.3	4
I_{cool} per beam (I_{sat})	14	14
$I_{\text{cool}}/I_{\text{rep}}$	8	20
D -line property	^{40}K	^6Li
$\Gamma/(2\pi)$ (MHz)	6.04	5.87
I_{sat} (mW/cm 2)	1.75	2.54

$\Delta \sim \max[\epsilon_{F=I+1/2}]$, $\Delta \sim -\max[\epsilon_{F=I-1/2}]$ are substantially suppressed.

III. SIMULTANEOUS ^6Li AND ^{40}K D_1 COOLING

Finally, we discuss the simultaneous operation of the ^6Li and ^{40}K D_1 molasses. We found that this simultaneous operation is required for subsequent efficient thermalization between both species in a quadrupole magnetic trap. The timing sequence and parameters are the same as for single-species operation. Experimental details are given in the Appendix and in [10]. The D_1 molasses phase is composed of a 3-ms capture phase and a 2-ms cooling phase. Table I summarizes the optimal parameters of the dual-species molasses. The presence of the other species reduces the atom numbers in the MOTs by 4% for ^6Li and by 10% for ^{40}K . However, we observe no mutual influence during the CMOT and the D_1 molasses phase. The temperatures and relative atom numbers in dual-species operation do not differ from those in single-species operation. There are several reasons for this. First, the D_1 resonances and lasers are ~ 100 nm apart in wavelength. Second, the CMOT and molasses phases are short in duration (5 ms) and the light-induced interspecies collision losses or heating are minimized as atoms are accumulated in dark states. Table II summarizes the performance of the different experimental

TABLE II. Performance of the different experimental phases for ^6Li and ^{40}K , in dual-species operation. We list the optimum temperature T , the atom number N , the density n , and the phase-space density ϕ .

	T (μK)	N (10^9)	n (10^{10} cm^{-3})	ϕ^a (10^{-5})
Lithium				
MOT	1000	2	2.6	0.03
CMOT	800	2	18	0.29
Molasses	48	1.2	7.6	8.2
Potassium				
MOT	240	3.2	7	0.02
CMOT	2000	3.2	37	0.06
Molasses	11	3.2	30	10.7

^aThe given phase-density does not take into account the different internal states and is calculated as $\phi = n\lambda_B^3$, where λ_B is the thermal de Broglie wavelength.

phases in dual-species operation. For both ${}^6\text{Li}$ and ${}^{40}\text{K}$ the D_1 molasses phase largely reduces the temperature, while the cloud size after the CMOT phase is conserved. For both species this leads to a phase-space density close to 10^{-4} .

IV. CONCLUSION

In this study we have investigated the properties of D_1 laser cooling both experimentally and with numerical simulations. The simulations take into account all relevant Zeeman and hyperfine levels as well as the 3D bichromatic lattice geometry. Simulations and experimental results match fairly well for both lithium and potassium. Various sub-Doppler cooling effects [10] are recovered in the full model. We have outlined the importance of coherences between the ground-state hyperfine levels [11] and interpreted the cooling mechanisms as resulting from a combination of VSCPT-like nonadiabatic transitions between dark and coupled states and Sisyphus-type cooling. The discrepancy (factor of 2 to 4) between the temperature predicted by the semiclassical model and the experimentally observed ones calls for further investigations and the development of a full quantum treatment of the external atomic motion using a Monte Carlo wave-function approach [15,29].

We have discussed the physics behind the robustness of the D_1 cooling scheme, in particular, its insensitivity to the excited-state hyperfine splitting and to the relative phase between the cooling and the repumping lattices, which is in sharp contrast to its D_2 counterpart [4,5,19]. We first suggest and numerically verify that, due to the predominance of the “open transitions” at D_1 , the bichromatically dressed ground states exhibit a robust correlation between light shift and decay. We clarify that such a correlation leads to the accumulation of an atomic population in the lowest energy dressed states at Raman resonance for both nonadiabatic and Sisyphus cooling. The picture also helps to explain the enhanced cooling at Raman resonance, as well as the reduced cooling or even heating at large Raman detunings. Because of the smaller absorption cross section for atoms cooled in weakly coupled states, D_1 gray molasses should also be less affected by the density-dependent heating than its D_2 counterpart [24].

Experimentally, using commercial semiconductor laser sources delivering ~ 200 mW of CW power, we achieve efficient, simultaneous cooling of ${}^6\text{Li}$ and ${}^{40}\text{K}$, resulting in a phase-space density close to 10^{-4} for both species. This D_1 cooling scheme enables efficient direct loading of a dipole or magnetic trap because of the large gain in temperature. As recently shown in [12] and [14], these conditions are well suited to direct loading of an optical dipole trap and to the performance of all-optical evaporation to quantum degeneracy. In our own experiments, we load a magnetic trap, transport the atoms to a separate science cell, and perform evaporative cooling of ${}^{40}\text{K}$ in two Zeeman states with a combined magnetic-optical trap scheme introduced in [25]. Deep quantum degeneracy ($T/T_F = 0.14$) in the dipole trap has been achieved and will be the subject of a future publication.

Finally, we have also used the D_1 gray molasses scheme to cool the bosonic ${}^{41}\text{K}$ isotope. All of 5×10^9 ${}^{41}\text{K}$ atoms from a CMOT were cooled to a final temperature of $20 \mu\text{K}$,

leading to a phase-space density of 1.1×10^{-4} . This confirms the generality of this D_1 sub-Doppler cooling method.

ACKNOWLEDGMENTS

We acknowledge useful discussions with A. T. Grier, I. Ferrier-Barbut, B. S. Rem, M. Delehaye, S. Laurent, and J. V. Porto and support from Région Ile de France (DIM Nano-K and IFRAF), the European Union (ERC grants Ferlodim and Thermodynamix), Institut de France (Louis D. Award), and Institut Universitaire de France. D.R.F. acknowledges the support of Fundação para a Ciência e Tecnologia (FCT-Portugal) through Grant No. SFRH/BD/68488/2010. S.W. acknowledges the support of the Physics Department at Swansea University, where part of this research was carried out.

APPENDIX: EXPERIMENTAL DETAILS

In this section we describe the experimental details, as well as the results of additional measurements on the D_1 molasses scheme, in particular, the single-species operation of ${}^6\text{Li}$. Our experimental setup has been described previously [18]. A Zeeman slower for ${}^6\text{Li}$ and a $2D^+$ MOT for ${}^{40}\text{K}$ load the 3D dual-species MOT in the MOT chamber. The D_2 laser systems for ${}^6\text{Li}$ and ${}^{40}\text{K}$ comprise master oscillator power amplifiers (MOPAs) to produce light at 671 and 767 nm, respectively. Beamsplitters and acousto-optic modulators generate the cooling and repumping beams, which are combined before injecting tapered amplifiers for the Zeeman slower and 3D MOT for ${}^6\text{Li}$ and, accordingly, the $2D^+$ MOT and 3D MOT for ${}^{40}\text{K}$.

The D_1 laser system for ${}^{40}\text{K}$ operates at 770 nm and is composed of a MOPA and an electro-optic modulator to produce the repumping frequency. The total power used for the ${}^{40}\text{K}$ cooling is 240 mW, with an intensity per molasses beam of $14I_{\text{sat}}$.

The source for the ${}^6\text{Li}$ D_1 light at 671 nm used in this work is a homemade solid-state laser, the next generation of [26] and [27], with up to 5 W output power. Acousto-optic modulators allow us to independently tune the frequencies and powers of the cooling and repumping beams, before recombination and injection into an optical fiber. We typically use 300 mW total power for the ${}^6\text{Li}$ D_1 cooling. The waist of the ${}^6\text{Li}$ D_1 beam after the telescope (Fig. 7) is 8.6 mm. We have also used a commercial 671-nm tapered amplifier system (MOPA) with 130 mW available power impinging on the atoms and obtained similar performances for the capture efficiency and sub-Doppler temperatures.

Our optical scheme superimposes the D_1 and D_2 light for both ${}^6\text{Li}$ and ${}^{40}\text{K}$ and produces the molasses and 3D MOT beams (Fig. 7). D-shaped mirrors (M_D) superimpose the D_1 cooling light and the 3D MOT light of each species before a dichroic mirror (M_{dichroic}) combines the lithium and potassium light. The beam containing all eight frequencies is expanded and distributed to the three pairs of $\sigma^+ - \sigma^-$ counter-propagating beams of the 3D MOT and the D_1 molasses. The two horizontal axes are retroreflected, and the vertical axis consists of two independent beams. The $\lambda/2$ plates of order 4 for lithium ($\lambda/2_{\text{Li}}^*$) and potassium ($\lambda/2_{\text{K}}^*$)

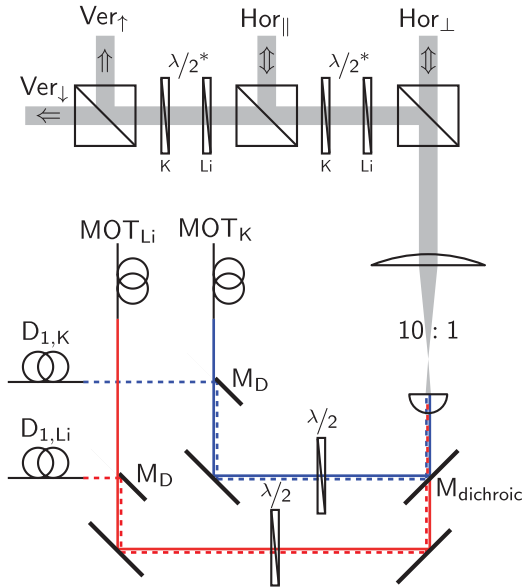


FIG. 7. (Color online) Optical scheme of the D_1 molasses. The 3D MOT light and the D_1 cooling light are superposed using a D-shaped mirror (M_D). Afterwards a dichroic mirror (M_{dichroic}) combines the lithium and potassium light, which is subsequently expanded and distributed to the three perpendicular axes of the 3D MOT.

allow for independent control of the ^6Li and ^{40}K MOT power distribution.

The experiment starts with the loading of the dual-species MOT. In 10 s we typically load 8×10^8 ^6Li atoms with an initial temperature of 1 mK and 3×10^9 ^{40}K atoms at $200 \mu\text{K}$. Then a CMOT phase [28] increases the density of the atom cloud. The magnetic gradient is linearly ramped from 9 to 60 G/cm in 5 ms. Meanwhile the frequencies of the cooling and the repumping beams are tuned closer to resonance and their intensities are linearly decreased. The CMOT phase results in an increase in the peak density by a factor of 7 (5.3) and a temperature of $800 \mu\text{K}$ (2 mK) for ^6Li (^{40}K). At the end of the CMOT phase the current of the MOT coils is switched off within $\sim 100 \mu\text{s}$. We start the D_1 molasses phase for ^6Li with a delay of $200 \mu\text{s}$ in order to wait for transient magnetic fields to decay. We found that this delay is not needed for ^{40}K .

1. ^6Li D_1 molasses

Here we study the cooling dynamics of ^6Li alone. We set the peak intensity of the molasses to $14.6I_{\text{sat}}$ per beam, set the cooling/repumping ratio to $I_{\text{cool}}/I_{\text{rep}} = 20$, and fix the global detuning to $\delta = \delta_{\text{cool}} = \delta_{\text{rep}} = 4 \Gamma$. Here $I_{\text{sat}} = 2.54 \text{ mW/cm}^2$ is the saturation intensity of the D_2 cycling transition, and $\Gamma = 2\pi \times 5.87 \text{ MHz}$ the D_1 line natural linewidth for ^6Li . Figure 8 shows the atom number and temperature of the D_1 molasses as functions of the molasses duration t_m . The temperature is determined through time-of-flight measurements. We capture 60% of the 8×10^8 CMOT atoms. Within 3 ms the atoms are cooled from $800 \mu\text{K}$ to the asymptotic temperature of $120 \mu\text{K}$ with a $1/e$ cooling time constant $\tau_{\text{cool}} = 0.6 \text{ ms}$. The direct

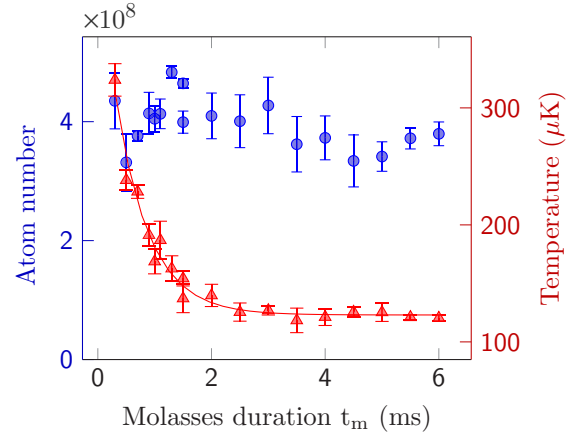


FIG. 8. (Color online) Number of atoms captured in the ^6Li D_1 molasses (circles) and their temperature (triangles) as functions of the molasses duration, with a $1/e$ cooling time constant $\tau_{\text{cool}} = 0.6 \text{ ms}$. The number of atoms in the compressed MOT is 8×10^8 .

measurement of the fluorescence shows a very fast decay at the beginning ($\tau_{\text{fast}} < 1 \mu\text{s}$), followed by a further decrease by another factor of 2 within 2 ms. This indicates that the atoms are accumulated in dark states during the cooling process. We find the $1/e$ lifetime of the D_1 molasses atom number for these parameters to be $\tau_{D_1} = 90 \text{ ms}$.

The molasses atom number and temperature as functions of the global detuning δ are shown in Fig. 9. We observe a decrease in the temperature from 188 to $100 \mu\text{K}$ for $\delta_{\text{cool}} = 2 \dots 7$. The capture efficiency increases sharply until 4Γ and stays constant until 7Γ .

We now study the influence of the D_1 light intensity. When increasing the cooling intensity, while keeping the molasses time fixed to 3 ms, we observe an increase in both the capture efficiency and the temperature (Fig. 10). To take advantage of the intensity-dependent temperature, we use two successive phases in the cooling sequence. During the first

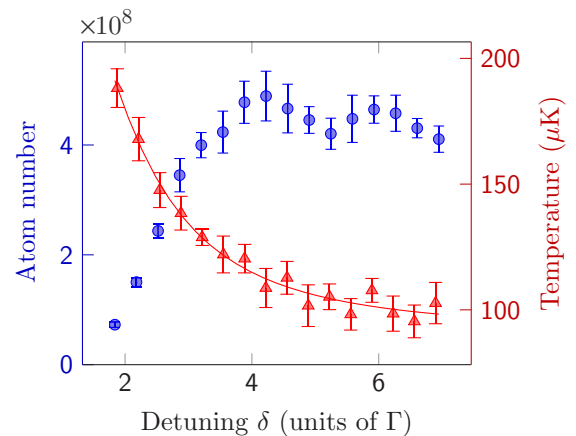


FIG. 9. (Color online) Number of atoms captured in the ^6Li D_1 molasses (circles) and their temperature (triangles) after a 3-ms capture phase at a high intensity, $I_{\text{cool}} = 14.6I_{\text{sat}}$, as functions of the global detuning $\delta = \delta_{\text{cool}} = \delta_{\text{rep}}$. The number of atoms in the compressed MOT is 8×10^8 .

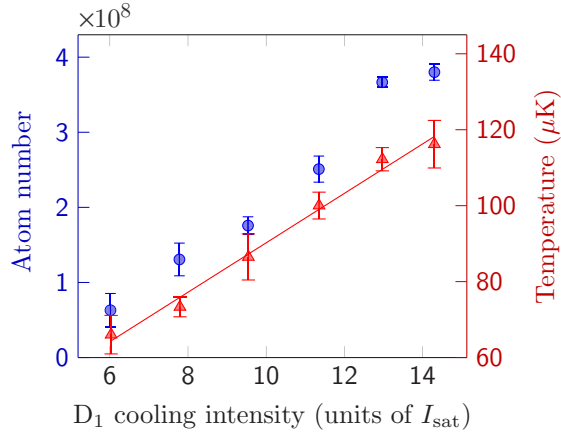


FIG. 10. (Color online) Number of atoms captured in the ${}^6\text{Li}$ D_1 molasses (circles) and their temperature (triangles) as functions of the D_1 cooling beam intensity for $\delta_{\text{cool}} = 4 \Gamma$ and $I_{\text{rep}} = I_{\text{cool}}/20$. The number of atoms in the compressed MOT is 8×10^8 . The atom number (temperature) increases linearly with a slope of 4×10^7 atoms/ I_{sat} ($6.5 \mu\text{K}/I_{\text{sat}}$).

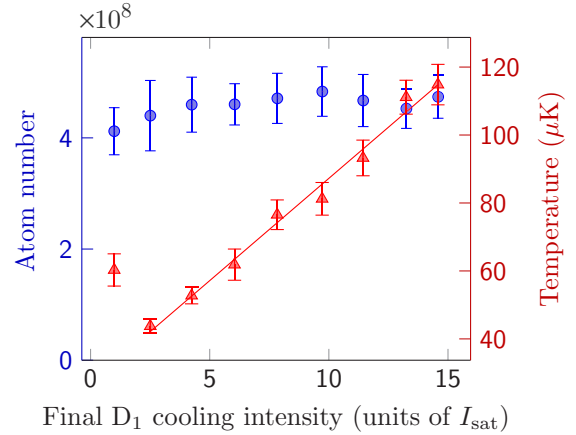


FIG. 11. (Color online) Number of atoms captured in the ${}^6\text{Li}$ D_1 molasses (circles) and their temperature (triangles) after a 3-ms capture phase at a high intensity, $I_{\text{cool}} = 14.6 I_{\text{sat}}$, followed by a 2-ms linear intensity ramp to an adjustable value. The temperature increases linearly for a higher intensity, with a slope of $\sim 6 \mu\text{K}/I_{\text{sat}}$. The detuning is fixed to $\delta_{\text{cool}} = 4 \Gamma$. The number of atoms in the compressed MOT is 8×10^8 .

3 ms we capture the atoms at a high intensity, yielding the highest capture efficiency. Then the intensity is linearly ramped within 2 ms to an adjustable final intensity to further lower the temperature. Figure 11 shows that the intensity ramp reduces the final temperature from 115 to 44 μK without a significant atom loss, for a final intensity $I_{\text{cool,final}} = 2.5 I_{\text{sat}}$. For lower intensities we observe heating and atom loss. The cooling/repumping intensity ratio influences the atom number and the temperature. We find an optimal temperature for $I_{\text{cool}}/I_{\text{rep}} = 20$. For a lower ratio the temperature increases

slightly and the atom number starts to drop at around $I_{\text{cool}}/I_{\text{rep}} = 7$. For $I_{\text{cool}}/I_{\text{rep}} > 33$ the cooling mechanism becomes inefficient, leading to atom loss and heating.

Measuring the atom cloud size at the end of the CMOT and molasses phases, we see no significant change, proving that diffusion during the molasses phase is small. In terms of the phase-space density the atom loss is largely overcompensated by the 14 times reduction in temperature.

-
- [1] J. Dalibard and C. Cohen-Tannoudji, *J. Opt. Soc. Am. B* **6**, 2023 (1989).
- [2] P. D. Lett, W. D. Phillips, S. L. Rolston, C. E. Tanner, R. N. Watts, and C. I. Westbrook, *J. Opt. Soc. Am. B* **6**, 2084 (1989).
- [3] D. S. Weiss, E. Riis, Y. Shevy, P. J. Ungar, and S. Chu, *J. Opt. Soc. Am. B* **6**, 2072 (1989).
- [4] A. Bambini and A. Agresti, *Phys. Rev. A* **56**, 3040 (1997).
- [5] X. Xu, T. H. Loftus, J. W. Dunn, C. H. Greene, J. L. Hall, A. Gallagher, and J. Ye, *Phys. Rev. Lett.* **90**, 193002 (2003).
- [6] P. Hamilton, G. Kim, T. Joshi, B. Mukherjee, D. Tiarks, and H. Müller, *Phys. Rev. A* **89**, 023409 (2014).
- [7] P. M. Duarte, R. A. Hart, J. M. Hitchcock, T. A. Corcovilos, T.-L. Yang, A. Reed, and R. G. Hulet, *Phys. Rev. A* **84**, 061406 (2011).
- [8] D. C. McKay, D. Jarvis, D. J. Fine, J. W. Simpson-Porco, G. J. A. Edge, and J. H. Thywissen, *Phys. Rev. A* **84**, 063420 (2011).
- [9] J. Sebastian, C. Gross, K. Li, H. C. J. Gan, W. Li, and K. Dieckmann, *Phys. Rev. A* **90**, 033417 (2014).
- [10] D. R. Fernandes, F. Sievers, N. Kretzschmar, S. Wu, C. Salomon, and F. Chevy, *EPL (Europhys. Lett.)* **100**, 63001 (2012).
- [11] A. T. Grier, I. Ferrier-Barbut, B. S. Rem, M. DeLahaye, L. Khaykovich, F. Chevy, and C. Salomon, *Phys. Rev. A* **87**, 063411 (2013).
- [12] G. Salomon, L. Fouché, P. Wang, A. Aspect, P. Bouyer, and T. Bourdel, *EPL (Europhys. Lett.)* **104**, 63002 (2013).
- [13] D. Nath, R. K. Easwaran, G. Rajalakshmi, and C. S. Unnikrishnan, *Phys. Rev. A* **88**, 053407 (2013).
- [14] A. Burchianti, G. Valtolina, J. A. Seman, E. Pace, M. De Pas, M. Inguscio, M. Zaccanti, and G. Roati, *Phys. Rev. A* **90**, 043408 (2014).
- [15] J. Dalibard, Y. Castin, and K. Mølmer, *Phys. Rev. Lett.* **68**, 580 (1992).
- [16] H. Carmichael, *An Open Systems Approach to Quantum Optics, Lecture Notes in Physics Monographs*, Vol. 18 (Springer-Verlag, Berlin, 1993).
- [17] By assuming the ground-state hyperfine splitting to be large enough, the $F = I + 1/2$ ($F = I - 1/2$) is dark to the repumping (cooling) laser and the associated couplings are ignored in the Hamiltonian. This approximation allows us to write down the Hamiltonian in the time-independent form.
- [18] A. Ridinger, S. Chaudhuri, T. Salez, U. Eismann, D. R. Fernandes, K. Magalhães, D. Wilkowski, C. Salomon, and F. Chevy, *Eur. Phys. J. D* **65**, 223 (2011).
- [19] R. Gupta, C. Xie, S. Padua, H. Batelaan, and H. Metcalf, *Phys. Rev. Lett.* **71**, 3087 (1993).
- [20] W. Happer, *Rev. Modern Phys.* **44**, 169 (1972).

- [21] C. Cohen-Tannoudji, *Atomic Motion in Laser Light*, edited by J. Dalibard, J. Raimond, and J. Zinn Justin (Les Houches, Session LIII, 1990), pp. 1–164.
- [22] Exact locations of the dark states depend on the relative phase between the cooling and the repumping lattices.
- [23] For D_2 transitions the complication is also Δ dependent. A complete comparison of D_1 and D_2 cooling will be the subject of a future publication.
- [24] M. Drewsen, P. Laurent, A. Nadir, G. Santarelli, A. Clairon, Y. Castin, D. Grison, and C. Salomon, *Appl. Phys. B* **59**, 283 (1994).
- [25] Y.-J. Lin, A. R. Perry, R. L. Compton, I. B. Spielman, and J. V. Porto, *Phys. Rev. A* **79**, 063631 (2009).
- [26] U. Eismann, F. Gerbier, C. Canalías, A. Zukauskas, G. Tréneç, J. Vigué, F. Chevy, and C. Salomon, *Appl. Phys. B* **106**, 25 (2011).
- [27] U. Eismann, A. Bergschneider, F. Sievers, N. Kretzschmar, C. Salomon, and F. Chevy, *Opt. Express* **21**, 9091 (2013).
- [28] M.-O. Mewes, G. Ferrari, F. Schreck, A. Sinatra, and C. Salomon, *Phys. Rev. A* **61**, 011403 (1999).
- [29] Y. Castin and K. Mølmer, *Phys. Rev. Lett.* **74**, 3772, (1995).